Interplay between long-range hopping and disorder in topological systems

Beatriz Pérez-González,[*] Miguel Bello,[†] Álvaro Gómez-León, and Gloria Platero
Instituto de Ciencia de Materiales de Madrid (ICMM), CSIC, 28049 Madrid, Spain

We extend the standard Su-Schrieffer-Heeger (SSH) model to include long-range hopping amplitudes and disorder, and analyze how the electronic and topological properties are affected. We show that long-range hopping can change the symmetry class and the topological invariant, while diagonal and off-diagonal disorder lead to Anderson localization. Interestingly, we find that the Lyapunov exponent $\gamma(E)$ can be linked in two ways to the topological properties in the presence of disorder—either due to the different response of midgap states to increasing disorder or due to an extra contribution to γ due to the presence of edge modes. Finally, we discuss its implications in realistic transport measurements.

I. INTRODUCTION

The dimer chain is a canonical model in condensed matter, widely used to study topological properties in atomic chains with staggered hopping amplitudes [1–7]. For the case of just nearest-neighbor hopping (NN), it reduces to the well-known SSH model [4]. However, the addition of long-range hopping amplitudes is important, as they are ubiquitous in real systems and their role can be crucial [8–10]. The effect of disorder in quantum systems can also be significant [11]. In topological systems in particular, its study has been focused on the change of the topological invariants [12–15]. However, its relation with localization has been typically overlooked, with some exceptions [16–19].

In this paper, we discuss the interplay between long-range hopping amplitudes and disorder in topological chains. We show that long-range hopping connecting sites within the same sublattice breaks chiral symmetry and changes the topological phase, leading to edge modes without the original topological protection. For large enough hopping amplitudes, the edge states mix with the bulk bands and the system becomes metallic. In contrast, long-range hopping amplitudes connecting different sublattice sites preserve chiral symmetry and allow us to increase the value of the topological invariant and the number of edge modes.

In the presence of disorder, Anderson localization happens. However, differences between diagonal (DD) and off-diagonal disorder (ODD) can be observed, when just NN hopping amplitudes are present due to the breaking of chiral symmetry in the first case but not the second. Furthermore, the localization properties for midgap and bulk states are different, and the Lyapunov exponent (LE) exhibits an extra contribution due to edge modes. This makes topology and localization intertwine in an interesting way. When next-nearest-neighbor (NNN) hopping amplitudes are included, the effect of both types of disorder is similar due to the lack of

chiral symmetry in both cases. However, it is possible to find signatures of topology in transport measurements, even deep within the metallic phase and for weak disorder.

II. MODEL

The standard SSH model is described in terms of noninteracting, spinless electrons populating a chain with alternating hopping amplitudes between neighboring sites. Its generalized Hamiltonian is

$$H_R = \sum_{|i-j| \leqslant R} (J_{i,j} + \epsilon_{i,j}) c_i^\dagger c_j + \text{H.c.}, \tag{1}$$

where $c_i^\dagger$ creates a fermion at the ith site and $J_{i,j}$, $i \neq j$, is the hopping amplitude connecting the ith and the jth sites. R is the maximum range of the hopping and we set $J_{i,i} = 0$. DD and ODD are introduced through $\epsilon_{i,j}$, for $i = j$ and $i \neq j$, respectively. For the numerical results, we have considered $\epsilon_{i,j} \in [-w/2, w/2]$ homogeneously distributed, although other choices are possible [20–22]. Because J_{ij} are functions of the distance $n = |i - j|$, to simplify our notation we separate hopping processes connecting sites within the same sublattice $J_{i,i\pm n} \equiv J_n$, with n even, and hopping processes connecting sites in different sublattices $J_{2i-n,2i} \equiv J_n$, and $J_{2i+n,2i} \equiv J_n'$, with n odd.

In absence of disorder, the Hamiltonian can be diagonalized in k-space and written in terms of the Pauli matrices as $\mathcal{H}_R = d_0(k)\mathbf{1} + \vec{d}(k) \cdot \vec{\sigma}$, with

$$d_0(k) = \sum_p 2J_{2p} \cos(pk), \quad d_z(k) = 0, \tag{2}$$

$$d_x(k) = \sum_p \{J_{2p-1}' \cos[(p-1)k] + J_{2p-1} \cos(pk)\}, \tag{3}$$

$$d_y(k) = \sum_p \{J_{2p-1} \sin(pk) - J_{2p-1}' \sin[(p-1)k]\}, \tag{4}$$

where $\mathcal{H}_R$ acts on the pseudospinor $\Psi_k = (a_k, b_k)^T$ and p ranges from 1 to $\lfloor (R+1)/2 \rfloor$ ($\lfloor \cdots \rfloor$ denotes the floor function). The dispersion relation is $E_\pm(k) = d_0(k) \pm |\vec{d}(k)|$,

[*]bperez03@ucm.es
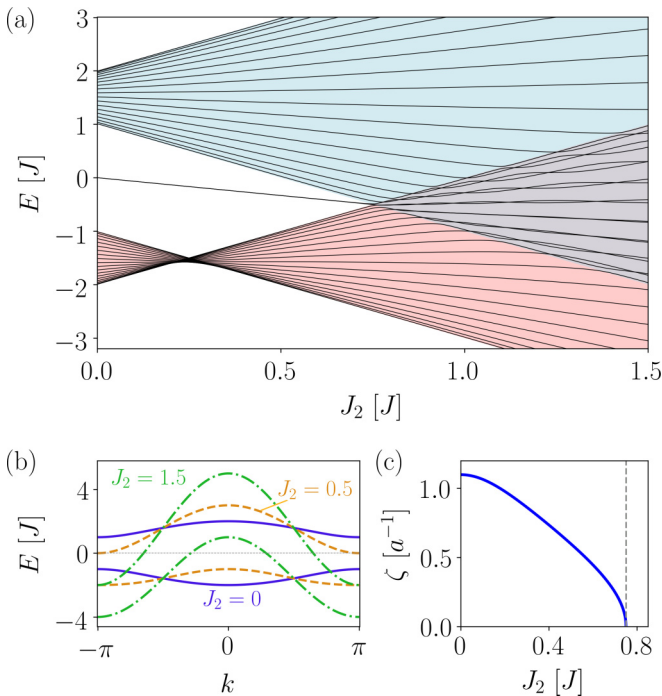[†]miguel.bello@icmm.csic.es

FIG. 1. Spectrum for a chain with up to NNN hopping. (a) Spectrum vs J_2 for a finite system with $N = 20$ unit cells. (b) Spectrum vs crystal momentum for different values of J_2. (c) Inverse of localization length vs J_2 for the edge states. All plots consider a chain with $\delta = -0.5$.

where $+$ and $-$ correspond to the conduction and valence band, respectively [see Fig. 1(b)].

III. ABSENCE OF DISORDER

The topological properties of the standard SSH model are captured with the Zak phase [23] or, equivalently, the winding number $\mathcal{W}$ of the Bloch vector $\vec{d}(k)$ [24].

As the SSH model has time-reversal, particle-hole, and chiral symmetry, it supports two distinct topological phases $|\mathcal{W}| \in \{1, 0\}$ featuring either a pair of edge states or none [25]. When longer-range hoppings are added, one can either break particle-hole and chiral symmetry if they connect the same sublattice (even hoppings) or preserve the symmetries if they connect different sublattices (odd hoppings). Even hoppings change the topological class from BDI to AI [26], while odd hoppings do not change the topological class and allow for larger values of the topological invariant [27]. Its maximum value is ultimately fixed by the range of the hoppings considered $|\mathcal{W}| \leqslant (R + 1)/2$. Finding a closed expression for $\mathcal{W}$ as a function of the system parameters is, in general, a hard task for couplings beyond NNN [28]. In Appendix A, we show how this can be done for first and third neighbors.

With arbitrary long-range hopping amplitudes, the system may still feature edge states, but there is not a one-to-one correspondence between the number of edge states and the topological invariant: The presence of even hopping introduces a term proportional to the identity matrix, which does not change the bulk eigenstates (leaving $\mathcal{Z}$ unaffected) but modifies the spectrum, making the bands overlap for sufficiently large values of the hopping amplitudes, changing the system

from insulating to metallic. This is seen in Fig. 1(a), where the spectrum, as a function of the NNN hopping amplitude J_2, makes the edge modes mix with the bulk bands when the single particle gap closes [8].

In a finite system, the presence of even hopping amplitudes also affects the spatial profile of the midgap states, as they do not come in chiral pairs anymore. Their localization length generally increases, diverging when they mix with the bulk bands. This can be seen already for NNN hopping: From perturbation theory, one can see that the energy of the edge states varies as $E_{\text{edge}} \simeq -2J_2 J_1'/J_1$. Then, looking for solutions of the dispersion relation with $k = \pi \pm i\zeta$, we obtain the following expression for the inverse of the localization length:

$$
\zeta = \frac{1}{\lambda_{\text{loc}}} = \text{acosh}\left[\frac{J_1'}{J_1} - \frac{J_1 J_1'}{4J_2^2} \right.
$$
$$
\left. + \frac{1}{4J_2^2}\sqrt{4J_2^2(J_1^2 - J_1'^2) + J_1^2 J_1'^2} \right], \quad (5)
$$

which is plotted in Fig. 1(c). There, the divergence of the localization length signals the transition to the metallic phase.

In the following, we focus on the effect of disorder, as well as on the transport properties with NNN present. For convenience, we reparameterize $J_1 = J(1 - \delta)$ and $J_1' = J(1 + \delta)$ in terms of the dimerization factor δ, and the average NN hopping amplitude J. In this convention, the topologically nontrivial (trivial) phase with $|\mathcal{W}| = 1$ ($|\mathcal{W}| = 0$) occurs for $\delta < 0$ ($\delta > 0$).

IV. DISORDER

DD modifies the on-site energies, and therefore acts within the same sublattice, breaking the chiral symmetry initially present in the standard SSH model. This modifies the topological phases, leads to a splitting of the zero-energy modes, and produces Anderson localization. On the other hand, ODD preserves chiral symmetry (well known for the Anderson model [21,22,29–31]) and keeps the topological phase well defined for weak disorder. In this case, the bulk electrons also localize but the edge states remain gapless until disorder is of the order of the dimerization factor $w \sim \delta$.

To gain insight into the localization properties in the standard SSH model, we have calculated a moment expansion of the LE [32]:

$$
\gamma_{\text{DD}}(E) \simeq \log|A| - \frac{E^2\sigma^2}{(E^2 - 4J^2)(E^2 - 4J^2\delta^2)}, \quad (6)
$$

$$
\gamma_{\text{ODD}}(E) \simeq \log|A| - \frac{h(E)\sigma^2}{2(A^2 - 1)^2 J_1^2 J_1'^2}, \quad (7)
$$

where

$$
A(E) = \left[f(E) \pm \sqrt{f(E)^2 - 4J_1^2 J_1'^2} \right] / 2J_1 J_1', \quad (8)
$$

$$
f(E) = E^2 - J_1^2 - J_1'^2, \quad (9)
$$

$$
h(E) = (A^4 - 8A^2 - 1)J_1^2 - 4A(A^2 + 3)J_1 J_1'
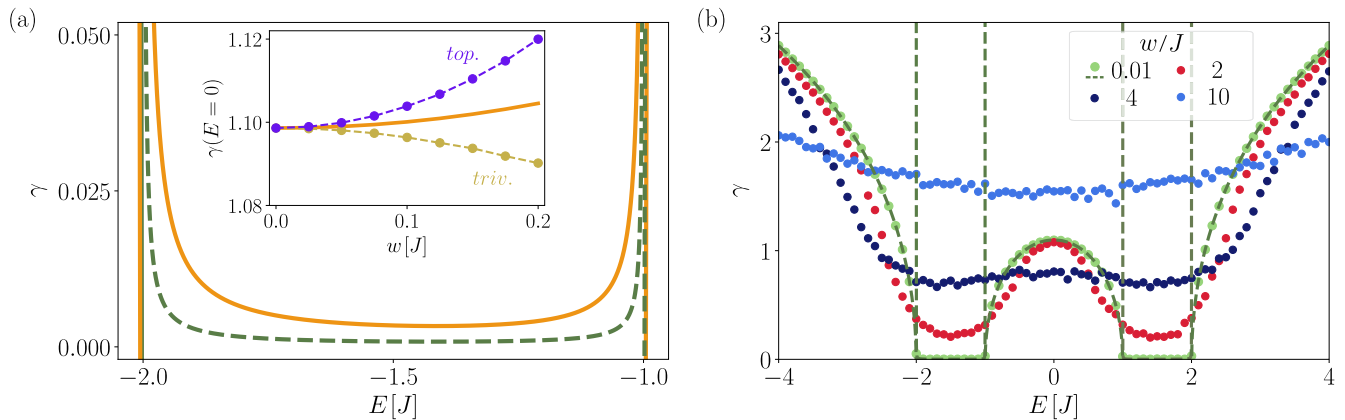$$
$$
+ (A^4 - 8A^2 - 1)J_1'^2. \quad (10)
$$

FIG. 2. (a) Comparison between γ_{DD} [Eq. (6), dashed green line] and γ_{ODD} [Eq. (7), orange line] for the states in the lower energy band with $\delta = -0.5$ and $w/J = 0.1$. Inset: Numerically calculated $\gamma_{\mathrm{ODD}}(E = 0)$ in the trivial (yellow dots) and topological (purple dots) phase as a function of the disorder strength w. The analytic formula Eq. (7) corresponds to the continuous orange line. (b) γ_{DD} vs E for different disorder strengths w in the SSH model. The dashed line (dark green) corresponds to the analytical approximation Eq. (6) and the dots to the numerical calculation. Parameters: $\delta = -0.5$.

(Details of the calculation can be found in the Appendix B.) Equation (6) corresponds to the case of weak DD, and Eq. (7) corresponds to the case of weak ODD. Figure 2(a) shows a comparison between the two analytic formulas. They display similar behavior, with the exception that ODD produces stronger localization. This is expected because values of the hopping amplitudes close to zero lead to full localization, and therefore disorder in the hopping amplitudes should produce stronger effects, for the same disorder strength.

Equations (6) and (7) recover the expressions for the Anderson model obtained by the same method: $\gamma(E) \propto -\sigma^2/(E^2 - 4J^2)$ in the limit $\delta \to 0$ (valid for both DD and ODD, being the prefactors the only difference between them). Importantly, as Eqs. (6) and (7) do not depend on the sign of δ, the trivial and topological phases cannot be distinguished by their localization properties for weak disorder, at least to second order in the perturbative expansion. This is not surprising because topological properties are not captured by local quantities.

Interestingly, due to the poles structure in Eqs. (6) and (7), there is a crossover region within the gap where localization is anomalous, changing sign for the states in the gap, which become less localized for increasing disorder. This is well-known in nontopological systems, but topological systems provide an extra twist: They display midgap states (only present in the topological phase) that delocalize as disorder increases, while the bulk states become more localized. This is important for measurements depending only on these mid-gap states, such as edge modes transport. Nevertheless, it is also important to keep in mind that structural defects such as impurities and dangling bonds can also produce these localized states within the gap. However, one could distinguish them with additional measurements, as, for example, testing the robustness of the topological states to remain at zero energy under small perturbations.

As a check, we have calculated numerically the Green's function $G = (E - H)^{-1}$ and by fitting the disorder-averaged elements $-\log(\langle G_{1,L} \rangle^2)$, $(L = 1, \ldots, 2N)$, we have obtained $\gamma(E)$ from its slope. Figure 2(b) shows the LE vs E for

different values of DD and a comparison with the analytical expression for weak disorder. The agreement is excellent and captures the previously discussed delocalization of midgap states. For large disorder, this phenomenon disappears and all states become more localized for increasing w, as typically observed in Anderson localization.

An interesting property, missing in the perturbative calculation, is shown in Fig. 2 (inset). It shows that the difference in $\gamma(E = 0)$ for the trivial and the topological phase, when ODD is added, is a nonvanishing function of the disorder strength (with variance always smaller than this difference). We have checked that this difference remains for different system lengths ($N = 50, 100, 150,$ and 200), which means that it should remain in the limit $N \to \infty$. Furthermore, this difference scales as σ^2, which would indicate that it does not correspond to higher orders in the perturbative expansion. Therefore, this evidence indicates that this contribution is a consequence of the presence of the edge modes.

When NNN hopping amplitudes are included, the electronic properties can be severely affected due to the changes in the energy bands, and especially due to the transition to a metallic phase with electron and hole pockets for large J_2. Figure 3 shows the value of $\gamma(E)$ for different values of J_2 and disorder. For small J_2, the chiral symmetry is weakly broken and the system still displays a gap, see Fig. 1. As J_2 increases, the bands and the LE become increasingly asymmetrical. It is interesting to see how DD and ODD disorder act in a similar way when NNN are present (purple and orange lines in Fig. 3). This is because chiral symmetry is already broken by J_2, and ODD also introduces fluctuations within the same sublattice [33]. For large J_2, the system becomes metallic and although the LE behaves similarly for DD and ODD, we demonstrate that transport in the trivial and in the topological phase can be quite different.

V. SINGLE-PARTICLE TRANSPORT

Coupling the ends of the SSH chain to voltage-biased leads allows for particle transport. We use second-order
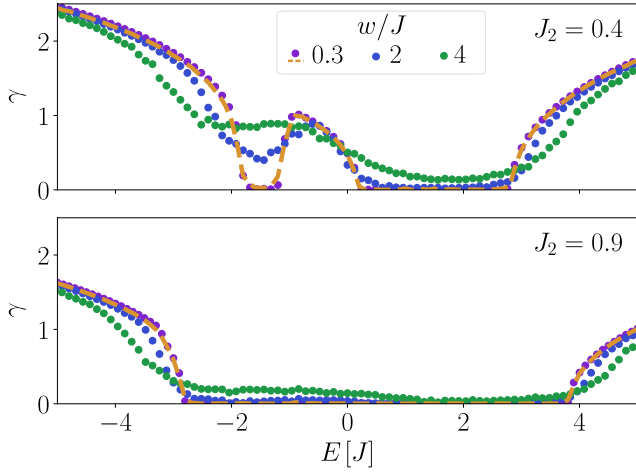
FIG. 3. Lyapunov exponent vs energy for a chain with fixed NN hopping amplitudes and different values of the NNN hopping amplitudes. The dots correspond to diagonal disorder, while the dashed orange line corresponds to off-diagonal disorder. Parameters: $\delta = -0.5$.

perturbation theory to integrate out the leads and obtain a master equation for the reduced density matrix of the chain ρ, which in the infinite bias regime assumes the following Lindblad form [7,34]:

$$\dot{\rho} = \mathcal{L}\rho \equiv -i[H_R, \rho] + \Gamma_L \mathcal{D}(c_1^\dagger)\rho + \Gamma_R \mathcal{D}(c_{2N})\rho, \quad (11)$$

where $\mathcal{D}(A)\rho \equiv A\rho A^\dagger - \{A^\dagger A, \rho\}/2$. The last two terms on the right-hand side of Eq. (11) correspond to incoherent tunneling of particles from the left lead into the first site of the chain at rate Γ_L, and tunneling out from the last site of the chain to the right lead at rate Γ_R.

We analyze transport, considering there is at most one particle in the system. This is the case if the interaction between particles inside the chain is strong enough such that higher chain occupancies are forbidden. The current in the stationary regime can be computed as $I = \text{tr}(\mathcal{J}\rho_0)$, where ρ_0 is the stationary solution of the master Eq. (11) and $\mathcal{J}\rho = \Gamma_L c_1^\dagger \rho c_1$ is the current superoperator.

In Fig. 4, we show the current in a pristine dimer chain with hopping amplitudes up to second neighbors as a function of the different hopping amplitudes. In the insulating regime in the topologically nontrivial phase ($\delta < 0$), we find the *topological edge-state blockade* already studied in Refs. [7,35]. As J_2 increases, the blockade remains up to the transition to the metallic phase. In the trivial region ($\delta > 0$), the current vanishes along the line $J_2 \simeq -\delta J/2 + J/2$, which corresponds to a configuration where the lower energy band is almost flat. For large enough J_2, the system is in the metallic phase and the current shows a pattern of dips in both the trivial and topological phases produced by exact crossings of energy levels with opposite parity (see the spectrum shown in Fig. 1). Whenever two states with opposite parity become degenerate, a superposition of both with zero occupation at the ending site of the chain becomes a steady state of the system. A particle in this superposition prevents any new particle from tunneling into the chain, and it cannot escape to the drain, thus blocking the current. Remarkably, most of these degeneracies occur
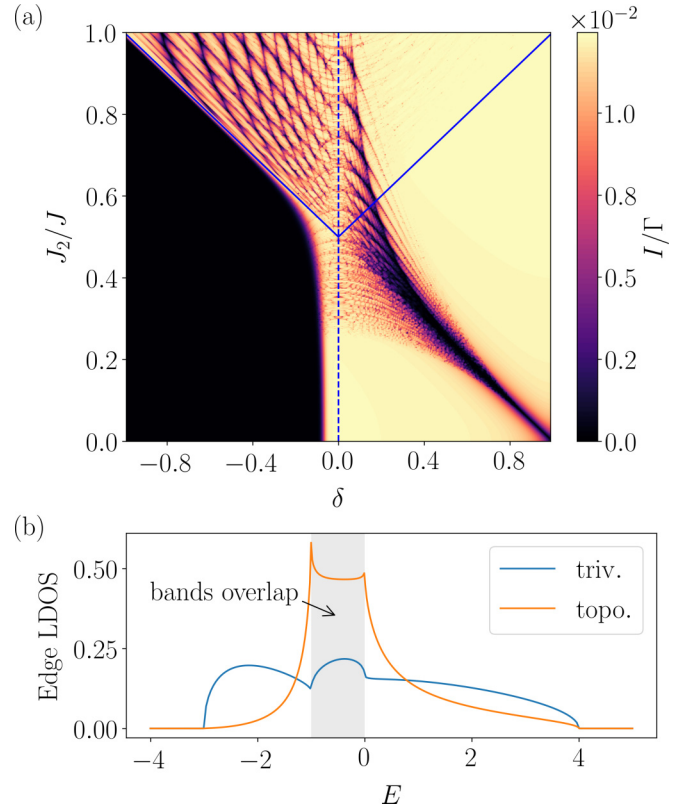

FIG. 4. (a) Current with $\Gamma_L = \Gamma_R = 0.1J$, for a chain with $N = 40$ dimers. The dashed vertical line marks the topological phase transition, while the upper triangle delimited by continuous lines marks the region where the system is metallic. (b) Local density of states at the ending site for a semi-infinite system with $J_2 = J$ and $\delta = -0.5$ (topological case) or $\delta = 0.5$ (trivial case).

for the same values of $|\delta|$ and J_2/J in the topological and trivial regimes. Nonetheless, most of the dips in the trivial region cannot be appreciated in Fig. 4 since they are much sharper than those in the topological regime (see Fig. 6 in Appendix C). The reason why resides in the way these states with opposite parity split near the degeneracy, and also in the relative weight they have on the ending sites of the chain as we demonstrate in Appendix C by analyzing a minimal model with three energy levels. This latter fact relates the local density of states at the ending sites of the chain [36], shown in Fig. 4(b), with the features observed in the current.

We have also computed the Fano factor, which is a measure of the shot noise in the transport process. Previous studies showed that for the standard SSH model, the Fano factor is approximately equal to 1 in the topological regime [7], meaning that transport is purely Poissonian. We find that for finite J_2 it is generally larger than 1 and presents clear differences between the topological and trivial phases. In the metallic region, it presents a characteristic peak-inside-a-dip shape at the exact crossings discussed above, that can again be related to the edge-local density of states (LDOS), as we show in Appendix C.

The effect of disorder on the current, when hoppings up to NNN are included, is similar for both DD and ODD, see Fig. 5. In the topological phase, near the exact crossings, the
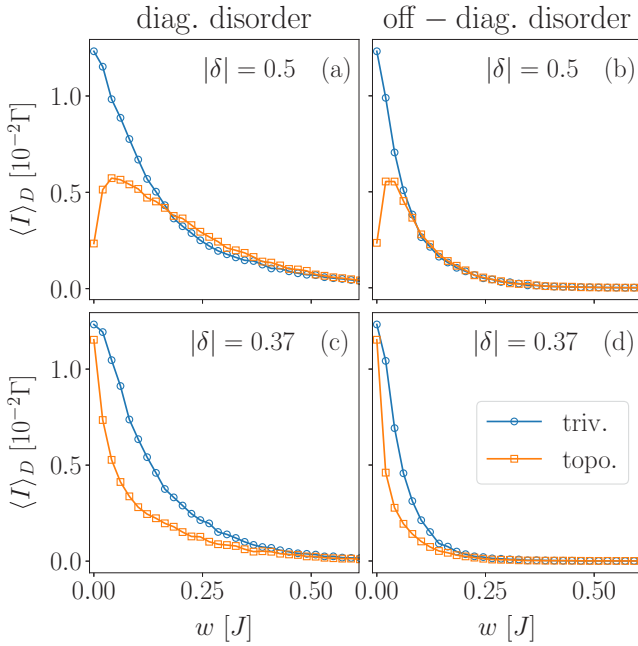
FIG. 5. Current as a function of the disorder strength for $J_2 = 0.9J$, $N = 40$, and $\Gamma_L = \Gamma_R = 0.1J$. Both diagonal (a), (c) and off-diagonal disorder (b), (d) is considered. The distribution of ϵ_{ij} is the same as the one used in the other figures. Each point has been obtained by averaging over a total of 10^3 instances of disorder. The parameters have been chosen such that on the upper plots, the current without disorder has a dip in the topological regime, while on the lower plots, the current shows a maximum in the topological regime.

current shows a nonmonotonic behavior, it increases for small disorder and decreases for large disorder. In the trivial phase, by contrast, the current decays monotonically with increasing disorder. This can be understood as follows: For zero disorder, near the exact crossings, the current is much smaller in the topological case than in the trivial, as it is carried mainly by almost-degenerate states with opposite parity, while in the trivial case it is carried equally by all states in the spectrum. Therefore, for small disorder, the current in the topological phase increases as disorder lifts the degeneracies that are blocking the current. On the other hand, in the trivial case the current decreases due to the increasing localization of the states. For large disorder, the current decreases in both phases as expected.

VI. CONCLUSIONS

We have studied a generalized SSH model including long-range hopping amplitudes and disorder. We have shown that the effect of hopping amplitudes connecting sites within the same sublattice, and those connecting sites of different sublattices is very different. The reason is that the former breaks particle-hole and chiral symmetry, changing the topological class, while the later maintains chiral symmetry and allows us to increase the value of the winding number. With both types of hopping processes, space inversion symmetry forces the topological invariant to have quantized values, but the bulk-edge correspondence breaks down. This is clear when NNN hopping amplitudes dominate, producing a metallic phase and the merging of the edge states with the bulk bands.

We have investigated the role of disorder using the LE. It shows that for NN hopping only, DD and ODD localize the bulk electrons, but their effect on midgap states is different, with a crossover from reduced to increased localization as a function of disorder strength. In addition, our numerical calculations find an extra contribution to $\gamma(0)$, as a function of ODD strength, that leads to a difference between the trivial and topological phase. This contribution is linked to the presence of edge modes. When NNN hoppings are added, chiral symmetry is broken and fluctuations in J_2 act similarly to DD. Nevertheless, we have shown that transport measurements for weak disorder can still distinguish between phases with different $\mathcal{W}$. Furthermore, the current in the metallic phase shows interesting features that also allow us to differentiate between them.

Our findings could be observed experimentally with arrays of quantum dots [37] in which the large Coulomb repulsion needed to keep at most one electron in the system could be engineered by capacitively coupling all dots together. In quantum dots, first-neighbor hoppings are of the order of 10 meV, while disorder strongly depends on the material and sample configuration.

Also, our results are relevant to the transport of excitations in analog systems, which could be implemented in platforms such as trapped ions [38] or cold atoms [39,40].

APPENDIX A: PHASE DIAGRAM WITH LONG-RANGE HOPPING AMPLITUDES

We derive here the phase diagram for a chain with up to fourth-neighbor couplings ($R \leqslant 4$). It only depends on the odd hopping amplitudes, i.e., on the ratios $x = J_1/J_1'$, $y = J_3'/J_1'$ and $z = J_3/J_1'$. The two-dimensional surfaces that delimit the regions with definite winding number are those points in parameter space for which the system of equations $d_x(k) = d_y(k) = 0$ has a solution for some $k \in [-\pi, \pi]$. These turn out to be the equations of two planes $P_1(x, y, z) = 0$, $P_2(x, y, z) = 0$, and a quadric $Q(x, y, z) = 0$, with

$$P_1(x, y, z) = 1 + x + y + z, \tag{A1}$$

$$P_2(x, y, z) = 1 - x - y + z, \tag{A2}$$

$$Q(x, y, z) = z - z^2 - xy + y^2. \tag{A3}$$

They divide the parameter space in finitely many regions. Computing the winding number inside each of these regions,

we obtain the whole phase diagram. For positive hopping amplitudes, the results are summarized in the following table (note that the plane P_1 does not appear):

$|\mathcal{W}|$	Conditions
0	($Q > 0$ and $P_2 > 0$) or ($Q < 0$, $P_2 > 0$ and $|y - x| > 2|z|$)
1	$P_2 < 1$
2	$Q < 0$, $P_2 > 0$ and $|y - x| \leqslant 2|z|$

APPENDIX B: CALCULATION OF THE LYAPUNOV EXPONENT

In the weak disorder limit, the analytic expressions for the LE can be obtained perturbatively from the equation of motion (EOM). This can be done by introducing the parameter $\lambda \ll 1$ in the disorder term as $E - \lambda \epsilon_m^\alpha$ (where α is the sublattice index, A and B), and $J_{ij} + \lambda \epsilon_{ij}$, for the diagonal and off-diagonal cases, respectively. As the SSH model is bipartite, each sublattice has an associated EOM, but they can be combined into a single one (for instance, for sublattice A).

By defining $R_m = a_m/a_{m-1}$, where a_m is the probability amplitude of the electronic wave function in the mth A-site of the chain, the LE can be written as

$$\gamma(E) = \lim_{M \to \infty} \frac{1}{M} \left\langle \sum_{m=1}^{M} \ln |R_m| \right\rangle, \tag{B1}$$

where is M is the number of cells in the chain and $\langle \cdot \rangle$ denotes configuration average. To find the LE, R_m can be expanded over the parameter λ in the following way:

$$R_m = A e^{\lambda B_m + \lambda^2 C_m + \lambda^3 D_m + \dots}, \tag{B2}$$

which in the limit $\lambda \ll 1$ yields

$$\gamma(E) = \lim_{M \to \infty} \frac{1}{M} \sum_{m=1}^{M} [\langle \ln |A| \rangle + \lambda \langle B_m \rangle + \lambda^2 \langle C_n \rangle + \dots]. \tag{B3}$$

By obtaining the leading orders of λ from the corresponding EOM, one can calculate $\langle \ln |A| \rangle$, $\langle B_m \rangle$, and $\langle C_n \rangle$. The λ^0 order of the combined EOM let us solve A as a function of the hopping amplitudes and energy, which yields the following result for both the DD and ODD cases:

$$A_{\pm} = \frac{E^2 - J_1^2 - J_1'^2 \pm \sqrt{\left(E^2 - J_1^2 - J_1'^2\right)^2 - 4J_1^2 J_1'^2}}{2 J_1 J_1'}, \tag{B4}$$

where A_- is valid within the band and the gap energy regions and A_+ outside the bands. This choice is necessary to ensure $\gamma(E)$ is positive for all E. Thus, $\gamma(E) = \lim_{M \to \infty} \frac{1}{M} \sum_{m=1}^{M} \langle \ln |A| \rangle$ defines the localization properties of the pristine SSH model. As expected, $\gamma(E)$ is zero within the energy bands and nonzero outside. Particularly, $\gamma(0) = 1/l = \log |J_1/J_1'|$ in the topological phase, which matches the well-known result for the localization length of the edge states [24].

Next, $\langle B_n \rangle$ can be obtained through the λ^1-equation upon averaging. For DD, we choose $\langle \epsilon_m \rangle = 0$ for both sublattices, as the chemical potential in the pristine system has been set to zero for all sites and the randomness induced by disorder is assumed to fluctuate around that value. For ODD, we set $\langle \epsilon_{ij} \rangle = 0$. In both cases, this results in a recursive equation for $\langle B_m \rangle$, which can be solved with $\langle B_m \rangle = 0$ without loss of generality.

Then, the $\langle C_m \rangle$ is calculated from the λ^2-equation after averaging. At this point, it is important to note that disorder, as introduced in the system, displays no correlations, and hence $\langle \epsilon_m^\alpha \epsilon_n^\beta \rangle = \delta_{\alpha\beta} \delta_{mn} \sigma^2$ for DD and $\langle \epsilon_{ij} \epsilon_{mn} \rangle = \delta_{ij} \delta_{mn} \sigma^2$ for ODD, where σ^2 is the standard deviation of the probability distribution followed by the random terms.

Finally, the LE can be written as $\gamma(E) = \ln |A| + \langle C_m \rangle$ for both cases. For DD, this yields

$$\gamma(A) = \ln |A| - \frac{A(AJ_1 + J_1')(J_1 + AJ_1')}{(A^2 - 1)^2 J_1^2} \sigma^2. \tag{B5}$$

For ODD, one obtains

$$\gamma(A) = \ln |A| + \left[\frac{(A^4 - 8A^2 - 1)J_1^2 - 4A(A^2 + 3)J_1 J_1'}{2(A^2 - 1)^2 J_1^2 J_1'^2} \right.$$
$$\left. + \frac{(A^4 - 8A^2 - 1)J_1'^2}{2(A^2 - 1)^2 J_1^2 J_1'^2} \right] \sigma^2. \tag{B6}$$

As a function of the energy, it is easy to compare the LE for ODD and DD cases,

$$\gamma_{\text{DD}}(E) = \ln |A| - \kappa(E)\sigma^2, \tag{B7}$$

$$\gamma_{\text{ODD}}(E) = \ln |A| - \kappa(E)\sigma^2 + \xi(E)\sigma^2, \tag{B8}$$

where

$$\kappa(E) = \frac{4E^2}{(4J^2 - E^2)(4J^2\delta^2 - E^2)}, \tag{B9}$$

and

$$\xi(E) = \frac{[8J^2\delta^2 - E^2(1 + \delta^2)]\sqrt{(4J^2 - E^2)(4J^2\delta^2 - E^2)}}{J^2(4J^2 - E^2)(4J^2\delta^2 - E^2)(\delta^2 - 1)^2}. \tag{B10}$$

The term $\xi(E)$ does not contribute in the band region, since the radicand is negative and hence the square root factor is imaginary.

APPENDIX C: ANALYSIS OF THE CURRENT AND FANO FACTOR

Explaining all the features the current and the Fano factor display is a hard task that requires knowledge of the full eigenbasis of the system. Here we attempt to give a qualitative understanding of the observed behavior near the exact crossings of the energy spectrum, which can be achieved considering a minimal single-particle model comprised of two almost-degenerate states with opposite parity $|\pm\rangle$ and a third level $|C\rangle$ which is highly detuned from the other two, such that it can be regarded as an exclusive channel for transport.

We can solve analytically the master equation for this small system noting that:
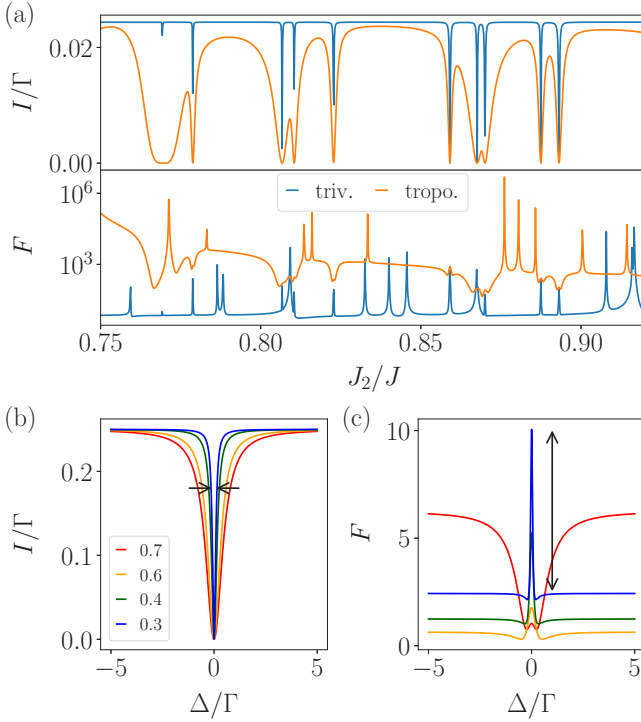
FIG. 6. (a) Current and Fano factor as a function of the NNN hopping amplitude for $\delta = \pm 0.5$, in the metallic region. The rest of the parameters are the same as in Fig. 4. (b), (c) Plot of the current and Fano factor in the minimal model for different values of $\alpha = \beta$ with $\Gamma_R = \Gamma_L \equiv \Gamma$. In (b), the width of the dip decreases as α^2 and β^2 become smaller (see black arrow). In (c), the height of the peak (black arrow) increases as α^2 and β^2 become smaller.

— The coherences between states with different numbers of particles evolve independently of the coherences between states with the same number of particles and the level populations.

— We can do a rotating-wave approximation in which we neglect coherences between eigenstates that are far off-resonance, that is, when their energy difference $(\epsilon_\mu - \epsilon_\nu) \gg \Gamma_{L,R}$.

Thus, in the particular model under consideration, to a good approximation we can include only the coherences between the $|\pm\rangle$ states. Apart from the splitting between these two states Δ, the other parameters that enter the master

equation are the weight of the states at the ending sites of the chain:

$$\langle 0| c_1 |+\rangle = \langle 0| c_{2M} |+\rangle = \alpha , \tag{C1}$$

$$\langle 0| c_1 |-\rangle = -\langle 0| c_{2M} |-\rangle = \beta , \tag{C2}$$

$$|\langle 0| c_1 |C\rangle| = |\langle 0| c_{2M} |C\rangle| = \sqrt{1 - \alpha^2 - \beta^2} . \tag{C3}$$

The parity of state $|C\rangle$ is irrelevant regarding the final result. Solving the master equation in the basis $\{|0\rangle \langle 0|, |+\rangle \langle +|, |-\rangle \langle -|, |+\rangle \langle -|, |-\rangle \langle +|, |C\rangle \langle C|\}$, ($|0\rangle$ denotes the vacuum state of the system) we obtain for the current:

$$I = \frac{\Delta^2 \Gamma_L \Gamma_R}{\Delta^2 (3\Gamma_L + \Gamma_R) + (\alpha^2 + \beta^2)^2 \Gamma_L \Gamma_R^2} . \tag{C4}$$

It goes from a finite value to zero when the states $|\pm\rangle$ become degenerate ($\Delta = 0$). Furthermore, the width of the dip is proportional to $(\alpha^2 + \beta^2)$. For the Fano factor, we will just give formulas for its value at $\Delta = 0$, and in the limit $\Delta \gg \Gamma_{L,R}$,

$$\lim_{\Delta/\Gamma_{L,R} \to 0} F = \frac{1}{2}\left(\frac{1}{\alpha^2} + \frac{1}{\beta^2} - 2 \right), \tag{C5}$$

$$\lim_{\Delta/\Gamma_{L,R} \to \pm\infty} F = 1 - \frac{6\Gamma_L}{3\Gamma_L + \Gamma_R} + \frac{2\Gamma_L \Gamma_R}{(3\Gamma_L + \Gamma_R)^2}$$
$$\times \left(\frac{1}{\alpha^2} + \frac{1}{\beta^2} + \frac{1}{1 - \alpha^2 - \beta^2} \right). \tag{C6}$$

They come in handy when analyzing the results shown in Fig. 6. First, the value of the Fano factor far from the resonances ($\Delta \gg \Gamma_{L,R}$) is minimal for the case $1/\alpha^2 = 1/\beta^2 = 1/3$, i.e., when all the single-particle states have equal weight on the ending sites of the chain. This explains why, on average, the Fano factor is larger in the topological phase than in the trivial, as the edge LDOS is much more regular in this latter case. Furthermore, the minimal model predicts the appearance of a peak in the Fano factor at the exact crossings, whose height relative to the base is given by $[-4 + 3/\alpha^2 + 3/\beta^2 - 1/(1 - \alpha^2 - \beta^2)]/8$ in the case $\Gamma_L = \Gamma_R$. It increases as the edge occupation of the states $|\pm\rangle$ decreases, which is also in accordance with the computed edge LDOS.

[1] R. E. Peierls, in *Quantum Theory of Solids*, Oxford Classic Texts in the Physical Sciences (Oxford University Press, Oxford, 1955).

[2] R. Jackiw and C. Rebbi, Phys. Rev. D **13**, 3398 (1976).

[3] W. P. Su, J. R. Schrieffer, and A. J. Heeger, Phys. Rev. Lett. **42**, 1698 (1979).

[4] W. P. Su, J. R. Schrieffer, and A. J. Heeger, Phys. Rev. B **22**, 2099 (1980).

[5] A. Gómez-León and G. Platero, Phys Rev. Lett. **110**, 200403 (2013).

[6] M. Bello, C. E. Creffield, and G. Platero, Sci. Rep. **6**, 22562 (2016).

[7] M. Benito, M. Niklas, G. Platero, and S. Kohler, Phys. Rev. B **93**, 115432 (2016).

[8] M. Di Liberto, D. Malpetti, G. I. Japaridze, and C. Morais Smith, Phys. Rev. A **90**, 023634 (2014).

[9] O. Viyuela, L. Fu, and M. A. Martin-Delgado, Phys. Rev. Lett. **120**, 017001 (2018).

[10] W. DeGottardi, M. Thakurathi, S. Vishveshwara, and D. Sen, Phys. Rev. B **88**, 165111 (2013).

[11] P. W. Anderson, Phys. Rev. **109**, 1492 (1958).

[12] C. W. Groth, M. Wimmer, A. R. Akhmerov, J. Tworzydło, and C. W. J. Beenakker, Phys. Rev. Lett. **103**, 196805 (2009).

[13] J. Li, R.-L. Chu, J. K. Jain, and S.-Q. Shen, Phys. Rev. Lett. **102**, 136806 (2009).

[14] G. Schubert, H. Fehske, L. Fritz, and M. Vojta, Phys. Rev. B **85**, 201105 (2012).

[15] E. V. Castro, M. P. López-Sancho, and M. A. H. Vozmediano, Phys. Rev. B **92**, 085410 (2015).

[16] T. Rakovszky and J. K. Asboth, Phys. Rev. A **92**, 052311 (2015).

[17] A. Altland, D. Bagrets, and A. Kamenev, Phys. Rev. B **91**, 085429 (2015).

[18] T. Liu and H. Guo, Phys. Lett. A **382**, 3287 (2018).

[19] P. Dutta, A. Saha, and A. M. Jayannavar, Phys. Rev. B **94**, 195414 (2016).

[20] T. Odagaki, Solid State Commun. **33**, 861 (1980).

[21] A. D. Stone and J. D. Joannopoulos, Phys. Rev. B **24**, 3592 (1981).

[22] C. M. Soukoulis and E. N. Economou, Phys. Rev. B **24**, 5698 (1981).

[23] J. Zak, Phys. Rev. Lett. **62**, 2747 (1989).

[24] P. Delplace, D. Ullmo, and G. Montambaux, Phys. Rev. B **84**, 195452 (2011).

[25] J. K. Asbóth, L. Oroszlány, and A. Pályi, *A Short Course on Topological Insulators: Band Structure and Edge States in One and Two Dimensions*, Lecture Notes in Physics Vol. 919 (Springer International Publishing, Cham, Switzerland, 2016).

[26] S. Ryu, A. P. Schnyder, A. Furusaki, and A. W. W. Ludwig, New J. Phys. **12**, 065010 (2010).

[27] B.-H. Chen and D.-W. Chiou, arXiv:1705.06913v4.

[28] L. Li, Z. Xu, and S. Chen, Phys. Rev. B **89**, 085111 (2014).

[29] L. Fleishman and D. C. Licciardello, J. Phys. C **10**, L125 (1977).

[30] H. Cheraghchi, S. M. Fazeli, and K. Esfarjani, Phys. Rev. B **72**, 174207 (2005).

[31] C. Zhou and R. N. Bhatt, Phys. Rev. B **68**, 045101 (2003).

[32] R. P. Budoyo, Conductance in mesoscopic rings, Ph.D. thesis, Wesleyan University, Connecticut, 2008.

[33] M. Inui, S. A. Trugman, and E. Abrahams, Phys. Rev. B **49**, 3190 (1994).

[34] H. Breuer and F. Petruccione, *The Theory of Open Quantum Systems* (OUP Oxford, Oxford, 2007).

[35] L. Ruocco and A. Gómez-León, Phys. Rev. B **95**, 064302 (2017).

[36] M. Möller, A. Mukherjee, C. P. J. Adolphs, D. J. J. Marchand, and M. Berciu, J. Phys. A: Math. Theor. **45**, 115206 (2012).

[37] D. M. Zajac, T. M. Hazard, X. Mi, E. Nielsen, and J. R. Petta, Phys. Rev. Appl. **6**, 054013 (2016).

[38] P. Nevado, S. Fernández-Lorenzo, and D. Porras, Phys. Rev. Lett. **119**, 210401 (2017).

[39] E. J. Meier, A. A. Fangzhao, A. Dauphin, M. Maffei, P. Massignan, T. L. Hughes, and G. Bryce, Science **362**, 929 (2018).

[40] L. Sanchez-Palencia and M. Lewenstein, Nat. Phys. **6**, 87 (2010).